From Single Element Complex B1 Mapping to Local SAR Estimation using Multi-channel Transceiver Coil at 7T

Xiaotong Zhang[1], Jiaen Liu[1], and Bin He[1]
[1]*Biomedical Engineering, University of Minnesota, Minneapolis, Minnesota, United States*

Introduction: Ultrahigh (UHF) MRI has been pursued with increasing interest [1]. While multi-channel transmit technique has been recognized as a potentially powerful tool for correcting B_1 inhomogeneities at UHF, management of the specific absorption rate (SAR), which is directly related to RF-induced heating, still remains one of the challenges faced by *in-vivo* UHF MRI applications [2]. Therefore, real-time and patient-specific local SAR estimation is highly desired in UHF MRI applications. Recently, the "Electrical Property Tomography (EPT)" technique has been pursued which uses electromagnetic theory to extract electrical property (EP) distribution *in vivo* from measured B_1 maps [3-7]. In this work, using a 16-channel transceiver head coil at 7T, based on previously proposed method [6,7], we report our simulation study from single element complex B_1 mapping for *in-vivo* local SAR estimation on a realistic geometry head model.

Theory: Using hybrid B_1-mapping techniques [8,9] and a multi-channel transceiver array coil, with measurable transmit B_1 magnitude ($\left|\tilde{B}_{1,k}^{+}\right|$, "~" denotes complex quantity), proton density (PD) biased receive B_1 magnitude ($PD\times\left|\tilde{B}_{1,k}^{-}\right|$) for each coil element, as well as relative B_1 phase between coil elements, we can reconstruct complex transmit and receive B_1 (their magnitudes and absolute phases) for each coil element [6,7]. Then applying Eq. (1), the logarithm-based inverse algorithm [7], with either complex transmit or receive B_1, the conductivity and relative permittivity can be reconstructed. By Eq. (2), the z-component of electric field for each coil element $\tilde{E}_{z,k}$ can be estimated, thus the local SAR can be estimated using Eq. (3) under the assumption that $\left|\tilde{E}_z\right|$ is the dominant component of electric field [10].

$$\begin{cases}\sigma=[2\nabla\left|\tilde{B}_1\right|\cdot\nabla\arg(\tilde{B}_1)/\left|\tilde{B}_1\right|+\nabla\cdot\nabla\arg(\tilde{B}_1)]/(\omega\mu_0)\\ \varepsilon_r=-\{(\nabla\left|\tilde{B}_1\right|\cdot\nabla\left|\tilde{B}_1\right|)/\left|\tilde{B}_1\right|^2-\nabla\arg(\tilde{B}_1)\cdot\nabla\arg(\tilde{B}_1)+\nabla\cdot[(\nabla\left|\tilde{B}_1\right|)/\left|\tilde{B}_1\right|]\}/(\omega^2\mu_0\varepsilon_0)\end{cases} \quad (1)$$

$$\tilde{E}_{z,k}=-j*(\partial\tilde{B}_{1,k}^{+}/\partial x-j\partial\tilde{B}_{1,k}^{+}/\partial y-\partial\tilde{B}_{1,k}^{-*}/\partial x-j\partial\tilde{B}_{1,k}^{-*}/\partial y)/\mu/\omega/(\varepsilon-j\sigma/\omega) \quad (2)$$

$$SAR\approx\sigma\left|\tilde{E}_z\right|^2/2\rho,\ \ (\left|\tilde{E}_z\right|>>\left|\tilde{E}_x\right|\ \text{or}\ \left|\tilde{E}_y\right|) \quad (3)$$

Methods: Simulation data was utilized to test above methods. ANSYS software (ANSYS Inc., PA, USA) was used to perform simulation of B_1 distributions in the human head at 300 MHz. The coil model design was reproduced from the elliptical 16-channel transceiver array [11]. A 120-slice realistic geometry head model consisting of 20 materials (e.g., cerebrospinal fluid [CSF], white matter [WM] and grey matter [GM]) with $2\times2\times2.5mm^3$ resolution was incorporated with proper isotropic EPs values at 300 MHz [8]. Software calculations were obtained with single coil element transmitting RF power. PD ratio images with proton density ratio assignment (i.e. PD_{CSF}:PD_{WM}:PD_{GM}=1:0.65:0.8) was used to multiply each $\left|\tilde{B}_{1,k}^{-}\right|$ image to mimic PD ratio biased receive B_1 magnitude.

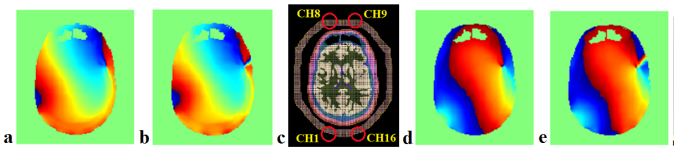

Fig.1: Target (a) and reconstructed (b) absolute phase of transmit B1, and target (d) and reconstructed (e) absolute phase of receive B1 for channel 3. 16 channels distributions is indicated in (c).

Results: (I) Channel 3 was chosen as the reference, and Fig.1 shows simulated and calculated absolute phase of transmit and receive B_1 for channel 3 on slice of interest: the calculated phase exhibiting a maximum of 0.24 radians difference and 0.993 in correlation coefficient (CC) when compared with simulated distribution. (II) The sagittal views, as well as five consecutive axial slices (S1-S5) of reconstructed EPs are plotted in Fig.2, showing 14%~21% relative errors (REs) and 0.931~0.978 CCs of reconstruction accuracy for tissues CSF, WM and GM. (III) Applying Eq. (2), we get 16 simulated and estimated $\left|\tilde{E}_{z,k}\right|$ on S3 (Fig.3) with average estimation RE of 29% and CC of 0.834. (IV) We arbitrarily chose element 4 for transmit, and Fig.4 depicts simulated (considering all three components of electric field) and estimated (considering only z-component of electric field) unaveraged local SAR distributions on coronal and axial slices of interest, respectively. Average RE of 38% and CC of 0.79 are observed between target and estimated SAR distributions.

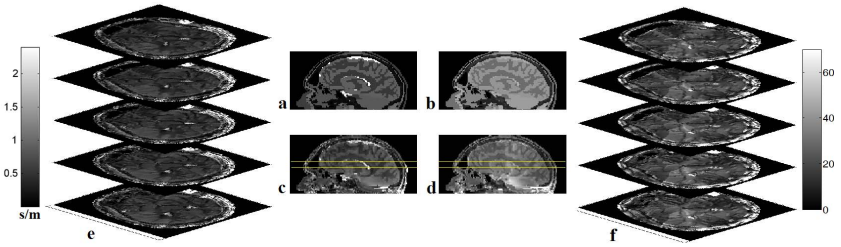

Fig.2: Sagittal views of target conductivity (a), target relative permittivity (b), reconstructed conductivity (c) and relative permittivity (d); reconstructed conductivity (e) and relative permittivity (f) on five consecutive axial slices within ROI (denoted in yellow).

Discussion and Conclusion: The previously developed method has demonstrated its capability of single element complex B_1 mapping using a multi-channel transceiver coil [6,7]. In the present study, promising simulation results suggest its feasibility and reliability of estimating local SAR for single transmit element. Future work involves experiment validation. Establishment of real-time EPT technique may have a significant impact on quantitative patient-specific SAR management in parallel transmission at UHF.

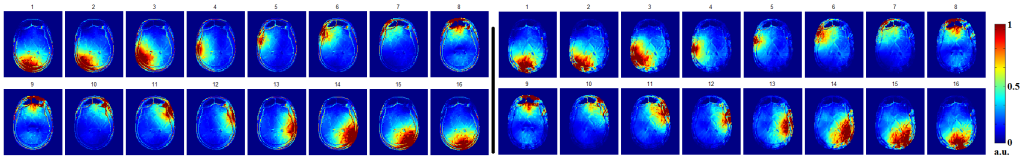

Fig.3: Magnitude of simulated (left) and calculated (right) z-component of electric field for each coil element.

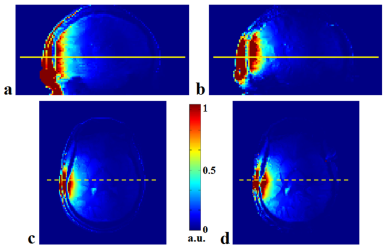

Fig.4: Choosing element 4 for transmit, the coronal views of target (a) and estimated (b) local SAR distributions, and the axial views of target (c) and estimated (d) local SAR distributions on the slices of interest, respectively. All SAR distributions are un-averaged.

References: [1] Ugurbil K et al., Magn Reson Imaging 2003(21):1263–1281. [2] Lattanzi R et al., MRM 2009(29):315-334. [3] Katscher U et al., IEEE TMI 2009(28):1365-1374. [4] Voigt T et al., MRM 2011(66):456-466. [5] Van Lier ALet al., MRM 2011. [6] Zhang XT et al., ISMRM 2011:126. [7] Zhang XT et al., submitted to MRM. [8] Van de Moortele PF et al., MRM 2005(54):1503-1518. [9] Van de Moortele PF et al., ISMRM 2007 :1676. [10] Cloos MA et al, ISMRM 2009:3037. [11] Adriany G et al., MRM 2008(59):590-597. **Acknowledgment:** NIH R01EB007920, R01EB006433, R21EB006070, and MSI at UMN. We are grateful to Dr. P.-F. Van de Moortele for providing the head geometry and coil models, and thank Dr. P.-F. Van de Moortele and Dr. S. Schimitter for useful discussions.